Sustainable Energy & Fuels

ROYAL SOCIETY OF CHEMISTRY

PAPER

View Article Online
View Journal | View Issue

Cite this: *Sustainable Energy Fuels*, 2025, **9**, 5627

Methanol-to-electricity *via* low-temperature steam reforming integrated with a high-temperature PEM fuel cell

Muhammad Aziz Ur Rehman, [a] Christian H. Schwarz,[a] Sina Souzani,[b] Christian Heßke[b] and Marco Haumann *[ac]

Liquid organic hydrogen carriers (LOHCs) are a promising method for renewable, green hydrogen transportation from the point of generation using renewable energy to the point of demand. Methanol is one such LOHC with advantages such as high hydrogen content, easy transportation and a simple reaction to release the hydrogen. Herein, we reported the use of a novel supported liquid phase (SLP) catalyst in a miniplant to carry out low-temperature methanol steam reforming (MSR) to release hydrogen and subsequently produce electricity using a high-temperature proton exchange membrane fuel cell (HT-PEMFC). This reformed methanol fuel cell (RMFC) setup successfully ran over the course of 45 h experiencing little catalyst deactivation, producing up to 49.2 l_N h^{-1} of hydrogen and up to 39 W electrical power using HT-PEMFC. Comparing between the reformate gas produced using SLP catalyst and pure hydrogen as feed for the fuel cell, the HT-PEMFC showed almost no difference in the voltage–current characteristic curve in the technically relevant operating points between 500 and 700 mV cell voltage. Furthermore, a pinch analysis indicated that the combination of a low-temperature MSR and HT-PEMFC presents an opportunity for heat-integration which could lead to increased efficiency.

Received 17th May 2025
Accepted 1st September 2025

DOI: 10.1039/d5se00703h

rsc.li/sustainable-energy

Introduction

Climate change remains an urgent global issue, requiring immediate strategies to prevent surpassing dangerous temperature thresholds.[1] With the current CO_2 levels exceeding targets required to minimize the impact of climate change, innovative solutions are critical.[1] Hydrogen has emerged as one of the most promising alternatives to conventional fossil fuels.[2] Despite its high gravimetric storage potential (120 MJ kg^{-1} for hydrogen *versus* 44 MJ kg^{-1} for gasoline), it has serious practical disadvantages: the very low volumetric energy density (8 MJ L^{-1} for $H_{2,liq}$ *versus* 32 MJ L^{-1} for gasoline) requires large, heavy, and expensive high-pressure tanks. Added to this are high infrastructure costs, energy-intensive compression, and demanding safety requirements.[3,4] The supply of externally produced, compressed hydrogen is recognized for its simple system architecture, but liquid organic hydrogen carriers LOHCs present an alternative way to transport hydrogen easily and safely. Methanol is one such promising LOHC, due to its high energy density, easy transportation, and potential for reducing CO_2 emissions when produced from renewable sources.[5–7] Hence, the use of liquid methanol as an energy carrier can ensure high volumetric energy density, easy storage, and a comparatively uncomplicated refueling infrastructure.

Methanol can be converted to electricity, by first, using MSR, where methanol and water react to form hydrogen and CO_2 (R1 in Scheme 1), and then hydrogen can be fed into conventional PEMFCs. Typically, copper-based heterogeneous catalysts are most commonly used for MSR, requiring high operational temperatures above 500 K.[8–10] However, this presents challenges, due to the high amounts of CO produced through methanol decomposition (reaction R2) shown in Scheme 1, which hence necessitates the purification of hydrogen due to its adverse effects on PEMFCs.[10,11] Although heterogeneous methanol steam reforming is well established, the higher operating temperatures lead to longer start-up times, higher energy requirements for the heating phase, and greater wear and tear. The plant design is more voluminous, thermal integration is more complex, making decentralized dynamic hydrogen supply difficult.

Recent advancements in catalyst development have introduced homogeneous catalyst complexes capable of operating under mild conditions (below 473 K), notably featuring transition metals such as Ru and Ir with pincer-type ligands.[12] Specifically, Ru-PNP pincer complexes (see Fig. 1) have demonstrated exceptionally high productivity (TON exceeding

[a]*Friedrich-Alexander-Universität Erlangen-Nürnberg (FAU), Lehrstuhl für Chemische Reaktionstechnik (CRT), Egerlandstr. 3, 91058 Erlangen, Germany. E-mail: marco.haumann@fau.de*

[b]*Zentrum für BrennstoffzellenTechnik (ZBT) GmbH, Carl-Benz-Str. 201, 47057 Duisburg, Germany*

[c]*Research Centre for Synthesis and Catalysis, Department of Chemistry, University of Johannesburg, P.O. Box 524, Auckland Park 2006, South Africa*

$$CH_3OH + H_2O \rightleftharpoons 3H_2 + CO_2 \qquad \Delta H = +49.6\ kJ\ mol^{-1}\ (R1)$$

$$CH_3OH \rightleftharpoons 2H_2 + CO \qquad \Delta H = +90.8\ kJ\ mol^{-1}\ (R2)$$

$$CO + H_2O \rightleftharpoons H_2 + CO_2 \qquad \Delta H = -41.3\ kJ\ mol^{-1}\ (R3)$$

Scheme 1 Reactions involved in methanol steam reforming including side reactions methanol decomposition (R2) leading to CO formation and water-gas shift reaction (R3).

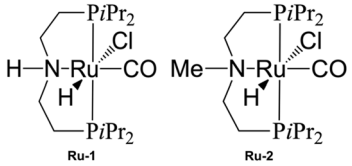

Fig. 1 Ruthenium-PNP pincer complexes, Ru-1 and Ru-2 immobilized in the BiCat SLP system.

350 000) and excellent long-term stability (lasting more than 3 weeks) in aqueous phase methanol reforming, while simultaneously maintaining low concentrations of CO (below 10 ppm).[13,14] This advancement addresses high CO formation and enhances the efficiency of the overall process due to lower temperature requirements.

Despite these benefits, scaling up the MSR using homogeneous catalysts is challenging. The corrosive environment due to the use of strong bases and carbonate buildup from CO_2 and base reactions can cause damage to the reactors and downstream processes. To overcome this, we have reported the use of a supported liquid phase (SLP) catalyst system for carrying out low-temperature MSR.[15,16] By immobilizing both the Ru-pincer complexes and the base on porous supports, the SLP catalyst avoids direct exposure of corrosive components to the reactor housing. Additionally, it confines carbonate formation, thereby extending catalyst longevity and operational stability. A bi-catalytic (BiCat) system using two different Ru-pincer complexes Ru-1 and Ru-2 is addressing the rate-determining steps in the consecutive reaction and thus enhances the overall efficiency.[17]

HT-PEMFC provide an optimal platform due to its high CO tolerance (approx. 1–2 vol%) and enhanced reaction kinetics due to elevated operational temperatures between 393 K and 453 K.[11] This simplifies the system design and reduces costs associated with hydrogen purification. This ability to directly use reformate gas from methanol offers significant advantages, promoting efficient co-generation and supporting diverse applications from stationary storage to transport.[5] This work explores for the first time the use of a RMFC system, which comprises of a low-temperature methanol reformer equipped with the BiCat SLP system to generate hydrogen and a HT-PEMFC to generate electricity from it. We assess its potential for efficient energy generation and the scope for heat-integration.

Experimental setup

Details of the SLP catalyst synthesis (1050 g) and characterization can be found in the SI. The RMFC system consisted of a miniplant used for the continuous low-temperature MSR coupled to a HT-PEMFC (see SI for details). Fig. 2 shows a simplified flow scheme of the setup used for the study. The evaporation of the reactants methanol and water was conducted without the use of a carrier gas and through thermal coupling with the fuel cell setup. The reactor (Halmosi GmbH, Heilbronn, Germany) provided about 2.5 L volume (length: 720 mm; inner diameter: 82 mm; material: 1.4571) and was heated *via* a two-zone heating jacket (Horst GmbH, Lorsch, Germany).

After the reactor, the product gas mixture was passed through the condenser to remove any unreacted methanol and water, and then the remaining mixture of H_2, CO_2, and CO entered the gas analyzer. The analyzer (X-STREAM Enhanced XEGP, Emerson Process Management GmbH & Co. OHG, Langenfeld, Germany) was equipped with a thermal conductivity detector (TCD) for hydrogen measurement and non-dispersive infrared (NDIR) photometers for CO and CO_2 detection (see Fig. A5 in SI). For H_2, the TCD offered a detection limit of $\leq$1 vol% with a configurable measurement range of 0–1% up to 0–100% H_2. CO_2 was measured by NDIR with a detection limit of $\leq$5 ppm and selectable ranges from 0–50 ppm up to 0–100% CO_2. CO was measured by NDIR with a detection limit of $\leq$10 ppm and ranges from 0–50 ppm up to 0–100% CO. These detector configurations provided low drift and fast response times, enabling accurate quantification of each gas species in the reformate stream under the specified operating conditions. After the gas analytics, the purified and quantified product gas could then be continuously fed into the fuel cell assembly, designed, and built for this application by The Hydrogen and Fuel Cell Center (Zentrum für BrennstoffzellenTechnik ZBT GmbH, Duisburg, Germany). An HT-PEMFC was selected for this coupling because it operates at a higher temperature range than the NT-PEMFC (423 K to 443 K), which results in higher tolerance to CO. A challenge with HT-PEMFC applications, however, is the temperature control due to the need for higher temperature durability of the materials used. For the selected HT-PEMFC concept, an appropriate novel cooling concept was developed and implemented. The selected thermal oil was pumped by the oil pump through the silicone hoses, entered a manifold pipe and was then directed to the part of the plant for hydrogen production from methanol, so that the waste heat from the HT-PEMFC could be used to support the conversion process.

Varying the flows of reactants into the reformer and process-related variations cause the amount of hydrogen produced to vary. This also changes the potential electrical current and electrical energy yield of the fuel cell. To control these fluctuations, the electronic load is operated in voltage-controlled

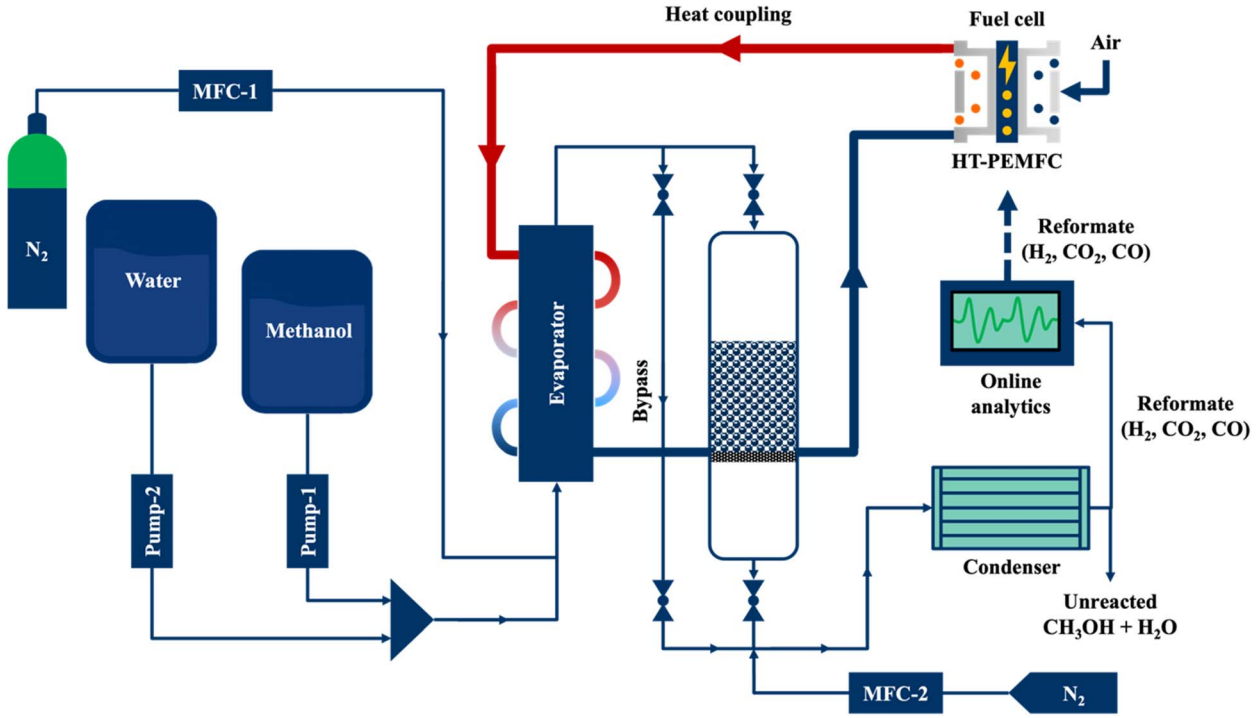

Fig. 2 Simplified flow scheme of the coupled RMFC. The pumps (pump-1 & pump-2) regulate the flowrate of the methanol and water, respectively. The MFCs (MFC-1 & MFC-2) regulate the flowrate of nitrogen inert gas. Reformate gas is analyzed using an Emerson XStream gas analyzer, equipped with detectors for hydrogen, carbon dioxide, and carbon monoxide gases. Red line indicates heat coupling between HT-PEMFC and evaporator *via* heat transfer fluid.

mode: it maintains a constant voltage at the fuel cell by automatically drawing as much current as is necessary and possible with the given hydrogen flow. The control algorithms required for this are integrated into the load. If the hydrogen supply increases, more current can be drawn at a constant voltage, thus generating more energy.

Results and discussion

In this study, a total of 1050 g of the BiCat SLP catalyst was used for the MSR. The catalyst was prepared in 200 g batches according to the synthesis procedure outlined in the SI. Because of this large amount, only a single experiment was carried out for stability and FC coupling testing. In previous experiments (eight individual runs) with smaller batches, a relative standard deviation of 6.7% was observed, indicative of good reproducibility of the activity (expressed as TOF). The gas composition is reproduced very consistently across all repetitions with a relative standard deviation of 0.08% over the course of the eight experiments.[18] The MSR reaction was operated at temperatures above 413 K to avoid condensation of the water vapor. To highlight the robustness of the BiCat SLP catalyst, the results for MSR obtained after a 350 h time on stream are presented in Fig. 3. In the initial 100 h time on stream, reaction parameters were varied to determine the optimal conditions for the system. The catalyst experienced small deactivation rates of about 0.13% h^{-1} which demonstrated the stability of the BiCat SLP catalyst along with high CO_2 selectivity. The main reason for the slow deactivation is a small loss of Ru and P as shown by post-run analysis of both the SLP catalyst as well as the condensed water-phase (see SI for details). No nanoparticles were detected by means of microscopy studies after the reaction and additionally, pore blocking can be ruled out, since the pore

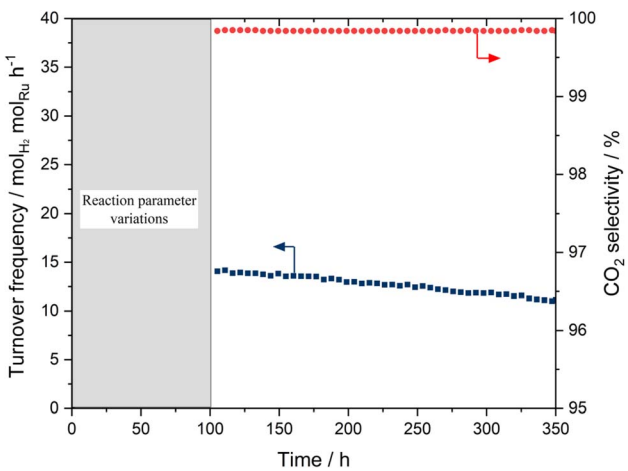

Fig. 3 Long-term activity (blue square, TOF) and CO_2 selectivity (red circle) in continuous methanol steam reforming on BiCat SLP catalyst. Reaction conditions: p = 0.1 MPa; n(MeOH: H_2O) = 1; T = 423 K; m_{cat} = 1050 g; GHSV = 40 h^{-1}. Catalyst composition: Φ_{Ru} = 50 μmol_{Ru} $g_{support}^{-1}$; $\Pi_{Ru\text{-}1\text{–}Ru\text{-}2}$ = 5.6; $\omega_{CsOH,syn}$ = 20 wt%; alumina support material 1.8 mm Ø.

Table 1 Comparison of MSR at low temperatures using Ru-SLP (this work) and selected, recently reported heterogeneous catalyst systems (publication year 2020–2024)

Catalyst	Mode[a]	T_{min}/K	X_{MeOH}/%	S_{H_2}/%	CO/ppm	TOS/h[b]	Ref.
Ru-pincer-SLP	FB	423	100	99.5	2000	250	This work
$Cu–MgO/Al_2O_3$	SE	523	100	99.3	<1500	10 cycles	19
Pt PN-CeO_2	APRM	333	99.1	100	0	—	20
$Pt/In_2O_3/CeO_2$	MR	573	>95	65	<4100	100	21
$Cu/Y_{1.5}Ce_{0.84}Ru_{0.04}O_4$	MR	573	99.5	98.7	1400	100	22
$Cu/MgAl_2O_4$	Mono	573	96	86	2800	30	23
$CuGa_2O_4$	FB	508	<60	>95	<100	50	24

[a] Mode refers to the reactor operation, where FB is fixed-bed, SE is sorption enhanced MSR, APRM is aqueous phase reforming, MR is micro-reactor, and mono is a monolithic reactor. [b] TOS is time-on-stream as stability measure.

morphology does not significantly change during reaction.[18] The CO concentrations reached about 400 ppm under these conditions (see Fig. S5 in SI). These results showed that a continuous operation of the RMFC would be possible to deliver a steady output of hydrogen which could be fed into the fuel cell.

To compare the MSR results using Ru-SLP catalyst with reported heterogeneous low-temperature systems, we compiled recent literature date in Table 1. From the data it is obvious that the Ru-SLP catalyst used in this work perform in a similar way compared to their heterogeneous counterparts, while the CO level is lower and the stability more than double.

The RMFC system, which integrated the reformer and fuel cell into one unit (see Fig. S2 to S4 in SI for details), was operated over the course of 45 h, and during that time, the catalyst experienced minimal deactivation as previously shown in the long-term test. Based on earlier catalyst tests, it was known that higher methanol content in the reactant increased hydrogen production. Therefore, the methanol to water molar ratio was varied from 2 : 1 to 4 : 1 to observe the resulting effect on the fuel cell performance. Fig. 4 shows the catalytic performance of the BiCat SLP catalyst, and the resulting electrical power generated from the fuel cell. Under these reaction conditions, CO levels reached well above 500 ppm. The amount of hydrogen produced increased from 36 to 49.2 $l_N\ h^{-1}$ due to the increase in methanol composition in the feed. The catalytic activity measured as TOF experienced a similar increase from just under 40 $mol_{H_2}\ mol_{Ru}\ h^{-1}$ to more than 50 $mol_{H_2}\ mol_{Ru}\ h^{-1}$. However, due to the higher methanol content in the feed, the CO_2 selectivity was negatively impacted from increased methanol decomposition reaction. The CO_2 selectivity declined from 99.7% (890 ppm CO) to 99.0% (2560 ppm CO). This increase in CO concentration also affected the fuel cell performance. At a hydrogen output of 36 $l_N\ h^{-1}$, the fuel cell generated about 33 W of electrical power but at increased hydrogen output of 49.2 $l_N\ h^{-1}$ only an increase to 39 W was seen. This is contrary to the 60 W that should be achievable with this hydrogen flow.

To further assess this decline in efficiency more precisely, faraday efficiency and electrical efficiency values were calculated. The faraday efficiency of the fuel cell corresponds to the amount of hydrogen which is converted to electrical energy. The electrical efficiency refers to the ratio of the measured power in

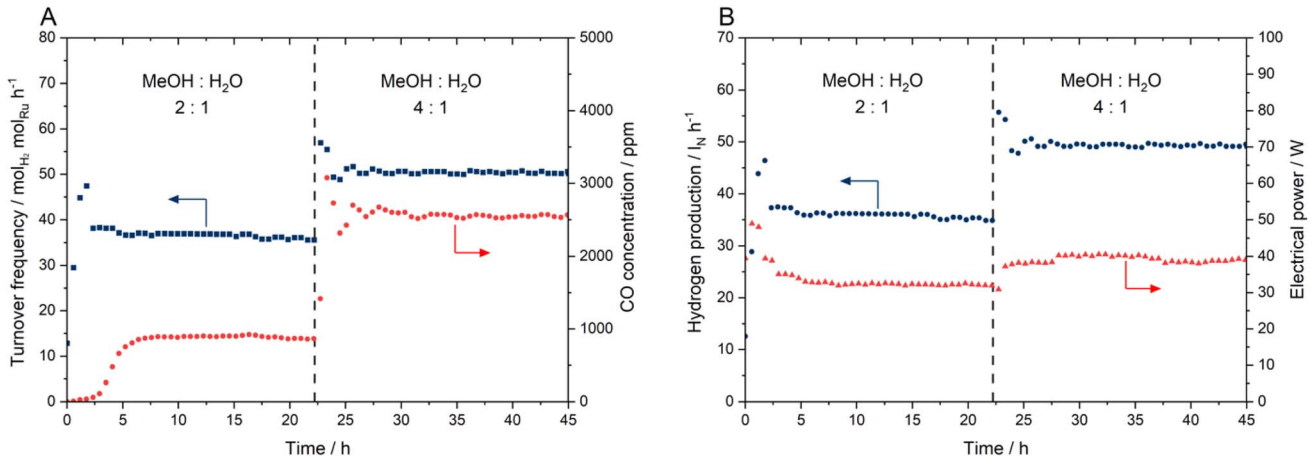

Fig. 4 Operation of the coupled RMFC system under two different reactant compositions of the reformer. (A) Activity (blue square, TOF) and carbon monoxide content in the product gas of the reformer (red circle) (B) hydrogen production rates (blue circle) on BiCat SLP catalysts; electrical power output of the HT-PEMFC (red triangle) in the coupled RMFC system. Reaction conditions: $p = 0.1$ MPa; $T = 423$ K; $m_{cat} = 1050$ g; GHSV = 110 − 180 h^{-1}. Fuel cell: $T = 423 - 443$ K; $\lambda_{O_2} = 2.5$; 6 cells with 50 cm^2 active area each. Catalyst composition: $\Phi_{Ru} = 50\ \mu mol_{Ru}\ g_{support}^{-1}$; $\Pi_{Ru\text{-}1-Ru\text{-}2} = 5.6$; $\omega_{CsOH,syn} = 20$ wt%; alumina support material 1.8 mm Ø.

Table 2 Characteristics of the reformate from continuous MSR using BiCat SLP catalyst and the HT-PEMFC in coupled operation

Parameter	Unit	Condition I	Condition II
$CH_3OH:H_2O$	—	2 : 1	4 : 1
$\dot{V}_{H_2}$	$l_N\ h^{-1}$ [a]	36	49.2
S_{CO_2}	% [b]	99.7	99.0
φ_{CO}	ppm [c]	890	2560
P_E	W [d]	33	39
P_T	W [e]	47	55
$\eta_{Faraday}$	% [f]	80	69
$\eta_{electrical}$	%	33	29

[a] Normal liters per hour at 0 °C and 1 bar. [b] Selectivity towards CO_2 in %. [c] Parts per million by volume. [d] Electrical power output in Watts. [e] Thermal power output in Watts. [f] Faraday efficiency, calculated as the ratio of the hydrogen converted to electrical current to the total hydrogen supplied. Equations used to obtain these values are listed in the SI. Reaction conditions: $p = 0.1$ MPa; $T = 423$ K; $m_{cat} = 1050$ g; GHSV = 110 − 180 h^{-1}. Fuel cell: $T = 423 - 443$ K; $\lambda_{O_2} = 2.5$; 6 cells with 50 cm^2 active area each. Catalyst composition: $\Phi_{Ru} = 50\ \mu mol_{Ru}\ g_{support}^{-1}$; $\Pi_{Ru\text{-}1-Ru\text{-}2} = 5.6$; $\omega_{CsOH,syn} = 20$ wt%; alumina support material 1.8 mm Ø.

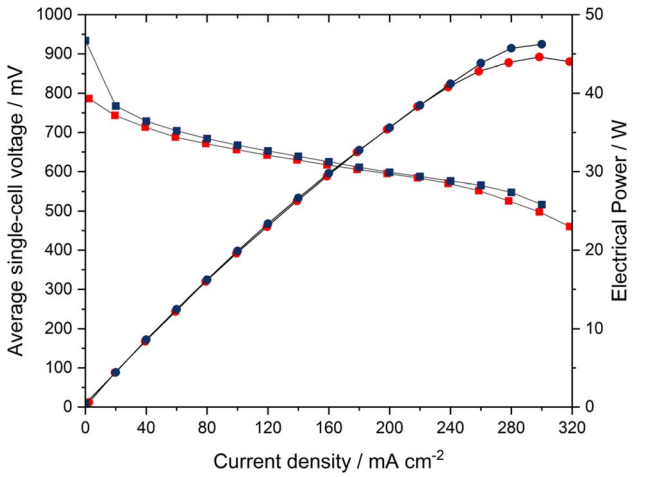

Fig. 5 Comparison of the *V–I* characteristics (squares) and power output (circles) of a HT-PEMFC setup with a 6-cell stack, operated with pure hydrogen (blue symbols) and reformate from the miniplant (red symbols). Fuel cell: $T = 423 - 443$ K; $Q_{H_2} = 800 - 900$ ml min^{-1}; 2560 ppm CO, 25% CO_2 in the reformate; $\lambda_{O_2} = 2.5$; 6 cells with 50 cm^2 active area each.

the fuel cell stack and the chemical potential of the energy carrier fed into the fuel cell. The energy carrier in this case is the hydrogen content of the product gas from the reformer. Not all the energy content of the hydrogen can be turned into usable energy, this results in electrical efficiency which is always below the faraday's efficiency. This loss in energy can be characterized by thermal power loss calculated from the difference in power from chemical conversion and the electrical power generated by the fuel cell. Table 2 lists all the characteristics of the MSR reaction and the HT-PEMFC under different methanol to water molar ratios.

As mentioned earlier, the shift of feed molar ratio from 2 : 1 to 4 : 1 results in a much lower increase in electrical power output of the fuel cell. This is indicated by the drop in faraday efficiency from 80 to 69% accompanied by a drop in electrical efficiency from 33 to 29%. This can be interpreted as poor utilization of a large portion of the hydrogen for electricity generation. Nevertheless, the system efficiency is in the range of modern HT-PEMFC setups reported in literature.[25] By varying the methanol molar ratio in the feed, several parameters are changed that have both a positive and negative influence on the voltage level of the fuel cell. These can lead to mixed potentials or kinetic inhibitions in the fuel cell, which reduces the effective efficiency.

The resulting increase in hydrogen volume flow has a positive effect on the H_2 partial pressure and thus on the voltage of the fuel cell. On the other hand, there is a sharp increase in the proportion of CO in the product gas. Despite the greatly increased CO tolerance of HT-PEM fuel cells compared to LT-PEM fuel cells, a concentration of 2.5% is already outside the range that can be tolerated in both short term and long term. This is because CO binds strongly to Pt anode surfaces and thus blocks active centres, leading to a drastic loss of catalyst activity.[26,27] Water in the product stream can promote CO removal through the water–gas shift reaction in the reformer gas, which has a rather mitigating effect on the catalyst poisoning. This positive influence disappears when the methanol molar ratio increases. Thus, the positive effect of the higher H_2 partial pressure is largely offset by the increasing CO poisoning. No influence on the proton conductivity of the membrane is to be expected, as it is primarily phosphoric acid that enables proton conductivity in HTPEM-BZ. In addition, the proportion of slip in unconverted methanol increases. This can damage the ionomer and thus reduce proton conductivity. However, this effect is more likely to occur in the medium term and is probably not yet apparent here.

To evaluate the effect of impurities in the reformate, the voltage–current characteristic curve was plotted to gain insights on the technical relevance of the RMFC system. The current intensity was varied at a constant volume flow of the reformate so that a corresponding cell voltage was produced. This was simulated with a comparable hydrogen flow without additional inert or harmful components and recorded for comparison. Fig. 5 shows the *V–I* characteristic curve and the plot of the electrical power over the current density. There was almost no difference observed for both the *V–I* and electrical power curves in the technically relevant operating points between 500 and 700 mV cell voltage. The main differences observed were a decrease of about 150 mV in the open circuit voltage and lower power output at 300 mA cm^{-2} when using reformate compared to pure hydrogen. The reduction in open circuit voltage is likely due to the hydrogen in the reformate being diluted with approximately 25 vol% CO_2. Additionally, the presence of CO contributes to mixed potentials at the anode, further reducing the voltage. However, despite impurities in the reformate, the RMFC system remained viable without experiencing any losses in the technically relevant voltages.

As seen earlier, the fuel cell experienced thermal losses of up to 55 W (see Table 2). This introduces an opportunity to utilize

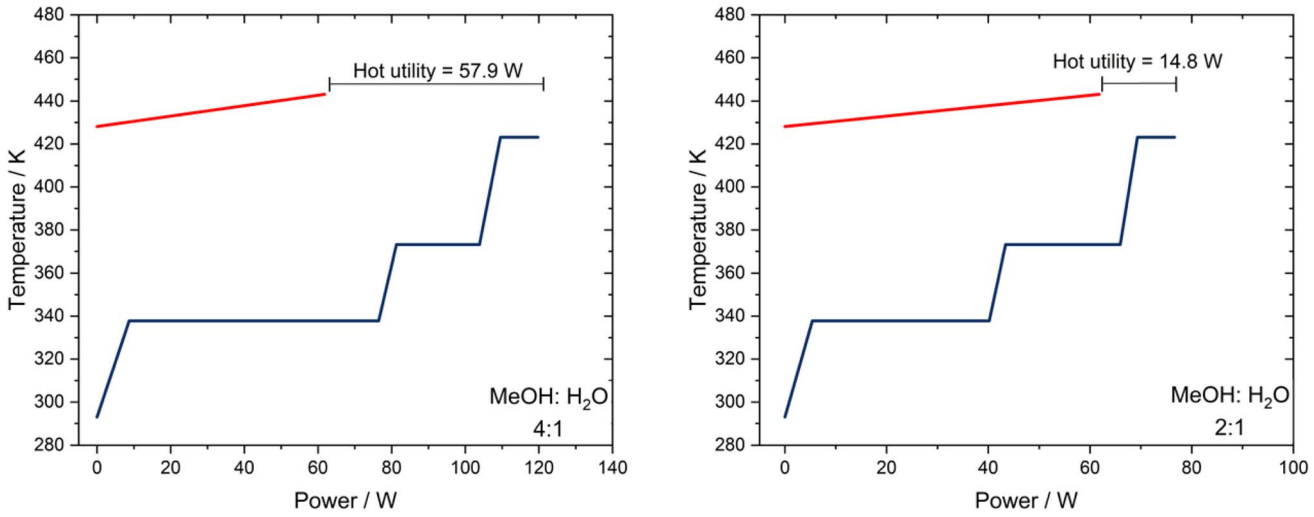

Fig. 6 Heat-integration between the waste heat of the fuel cell (red, hot stream) and the heat required to operate the methanol reformer (blue, cold stream) using the pinch method under different molar ratios of the feed. Reaction conditions: T = 423 K; $\dot{m}_{Methanol}$ = left: 3.7 | right: 1.9 g min^{-1}; $\dot{m}_{Water}$: 0.6 g min^{-1}; fuel cell: T = 443 K; $\dot{m}_{Fragoltherm}$: 120 g min^{-1}.

the waste heat for methanol reforming process through heat coupling. The fuel cell operates at temperatures between 423 and 443 K and can serve as a robust heat source due to the exothermic nature of the reactions. In contrast, the methanol reformer, operating at 423 K, functions as a heat sink due to the endothermicity of MSR reaction and the energy required for the evaporation of reactants. A suitable heat coupling would significantly improve the efficiency of the RMFC system and reduce overall energy consumption. Therefore, the RMFC system was integrated with a heat transfer medium which could transport waste heat from the periphery of the fuel cell and the exhaust gases to the evaporator. However, since the current setup comprised of a smaller scale HT-PEMFC, its heat energy output was relatively low, making it challenging to achieve heat coupling.

Although not feasible in the current setup, a successful implementation remains possible if this system can be applied in a larger scale. We can evaluate the potential for heat recovery using a pinch analysis. In this analysis, the hot stream, or heat source, is identified as the waste heat carried by the heat transfer medium from the fuel cell. While the cold streams, or heat sinks, are the heat inputs necessary for the evaporator to vaporize the reactants and the energy required for the MSR reaction based on the reaction enthalpy. For simplicity, heat losses were neglected from the calculation. SI lists the equations, Eq. (A.10) to (A.12), used for calculation of the heat-integration.

Based on the evaluation, 15 to 58 W power must be supplied as hot utility to the cold stream depending on the molar ratios of the feed (see Fig. 6). An excess of methanol in the feed leads to a significantly larger requirement for the hot utility as more methanol needs to be vaporized. We saw up to 37% conversion of water achieved using the BiCat SLP catalyst but even at 100% conversion, almost 75% of the methanol would remain unreacted, thus lowering the heat recovery benefits. Preferably, stoichiometric ratios of the reactants along with high conversions are required for the most efficient heat recovery.

We can also look at an ideal case, where water conversion reaches 90% due to MSR and this can be achieved by adjusting the reactant flow rates while keeping the experimental parameters of the fuel cell unchanged. Thermodynamically, this consideration is valid as conversions over 90% are possible under these reaction conditions.[28] However, a slowdown of the kinetics should be expected, and this was not considered. Such an improvement could be achievable by using a more active SLP catalyst, which is currently under development. In this scenario, the entire waste heat generated by the fuel cell could be utilized at the reformer and the evaporator. Instead of hot utility, a cold utility of 9 to 31 W would be required for cooling the fuel cell (see Fig. S6 in SI for details). However, due to heat losses always present in real systems, excess cooling power is technically advantageous. This effectively demonstrates that integrating a low-temperature MSR with a HT-PEMFC can result in an efficient RMFC system. The feasibility of such a system depends on the utilization of low-temperature SLP catalysts which make it possible to operate the reformer at much lower temperatures around 423 K than is conventionally possible.

Conclusion

In this study, a RMFC system using a novel BiCat SLP catalyst for low-temperature methanol steam reforming was employed to generate electricity. The BiCat SLP catalyst exhibited remarkable stability, maintaining minimal deactivation rates after continuous operation over 45 h. Notably, the HT-PEMFC integrated in the system remained operational producing a steady power output as high as 39 W. The efficiency of the fuel cell was influenced by the reformer feed composition. Increasing the methanol molar ratio in the feed increased catalytic activity and hydrogen production, and thus the

electrical power output. However, due to increased methanol decomposition, CO concentrations increased, and it resulted in lower-than-expected electrical power output despite the enhanced hydrogen flow rate. This was due to a decline in faraday and electrical efficiencies. Nevertheless, despite the presence of impurities in the reformate gas from catalyst degradation, uncondensed methanol and water and presence of CO, the HT-PEMFC remained functional without significant voltage losses within the technically relevant cell voltages of about 500 and 700 mV. Furthermore, heat-integration between the fuel cell and the reformer was shown to enhance efficiency by utilizing waste heat from the fuel cell during the reforming process. This could be particularly useful in pairing a low-temperature reformer using BiCat SLP catalyst with a HT-PEMFC. To further improve the overall efficiency of the heat-integration system, it is essential to enhance the catalytic activity of the BiCat SLP catalyst in future work. This will improve the efficiency of the heat-integration process, paving the way for its practical implementation in real-world scenarios. When considering the further scale-up of this combined RMFC setup, the catalyst particle size must be adjusted to the larger reactor device, and the pressure drop must be considered. In unpublished studies, we have successfully utilized SLP catalysts up to *xxx* mm without encountering transport or pressure drop limitations. For continuous operation, it is advisable to plan staged, modular reactors to ensure high on-stream factors during necessary changeouts.

In summary, low-temperature methanol steam reforming-H_2 system offers a quick system start-up and compact, easily integrable reactor designs due to its very low reaction temperature. It also has potential for highly efficient, decentralized power supply. Despite the challenges of high-quality catalysts and precise process control, these challenges also open up scope for cost reductions and efficiency improvements in future generations. Small-scale applications are likely to be addressed at the current stage of development.

Author contributions

M.A.U. Rehman – visualization, writing; C.H. Schwarz – conceptualization, formal analysis, validation, visualization; S. Souzani – formal analysis, visualization; C. Heβke – supervision, validation, funding acquisition; M. Haumann – supervision, funding acquisition, writing.

Conflicts of interest

The authors declare no conflict of interest.

Data availability

The data that support the findings of this study are available from the upon reasonable request.

Supplementary information: Detailed nomenclature, catalyst synthesis and characterization, in detail description of reactor setup and operation, and information on spent SLP catalyst analysis. See DOI: **https://doi.org/10.1039/d5se00703h**.

Acknowledgements

The research leading to these results has received funding from the German Federal Ministry of Economic Affairs and Energy (BMWi) within the projects Metha-Cycle (grant number 03ET6071) and MEGA (grant number 03EN5006). The authors thank Sasol Germany for providing the support pellet samples.

References

1 J. Hansen, P. Kharecha, M. Sato, V. Masson-Delmotte, F. Ackerman, D. J. Beerling, P. J. Hearty, O. Hoegh-Guldberg, S.-L. Hsu, C. Parmesan, J. Rockstrom, E. J. Rohling, J. Sachs, P. Smith, K. Steffen, L. Van Susteren, K. von Schuckmann and J. C. Zachos, Assessing "Dangerous Climate Change": Required Reduction of Carbon Emissions to Protect Young People, Future Generations and Nature, *PLoS One*, 2013, **8**, e81648, DOI: **10.1371/journal.pone.0081648**.

2 S. Dunn, Hydrogen futures: toward a sustainable energy system, *Int. J. Hydrogen Energy*, 2002, **27**, 235–264, DOI: **10.1016/S0360-3199(01)00131-8**.

3 P. Nikolaidis and A. Poullikkas, A comparative overview of hydrogen production processes, *Renew. Sustain. Energy Rev.*, 2017, **67**, 597–611, DOI: **10.1016/j.rser.2016.09.044**.

4 A. M. Abdalla, S. Hossain, O. B. Nisfindy, A. T. Azad, M. Dawood and A. K. Azad, Hydrogen production, storage, transportation and key challenges with applications: A review, *Energy Convers. Manag.*, 2018, **165**, 602–627, DOI: **10.1016/j.enconman.2018.03.088**.

5 S. Simon Araya, V. Liso, X. Cui, N. Li, J. Zhu, S. L. Sahlin, S. H. Jensen, M. P. Nielsen and S. K. Kær, A Review of The Methanol Economy: The Fuel Cell Route, *Energies*, 2020, **13**, 596, DOI: **10.3390/en13030596**.

6 P. T. Aakko-Saksa, C. Cook, J. Kiviaho and T. Repo, Liquid organic hydrogen carriers for transportation and storing of renewable energy – Review and discussion, *J. Power Sources*, 2018, **396**, 803–823, DOI: **10.1016/j.jpowsour.2018.04.011**.

7 F. Schorn, J. L. Breuer, R. C. Samsun, T. Schnorbus, B. Heuser, R. Peters and D. Stolten, Methanol as a renewable energy carrier: An assessment of production and transportation costs for selected global locations, *Adv. Appl. Energy*, 2021, **3**, 100050, DOI: **10.1016/j.adapen.2021.100050**.

8 M. A. Achomo, A. Kumar, N. R. Peela and P. Muthukumar, Hydrogen production from steam reforming of methanol: A comprehensive review on thermodynamics, catalysts, reactors, and kinetic studies, *Int. J. Hydrogen Energy*, 2024, **58**, 1640–1672, DOI: **10.1016/j.ijhydene.2024.01.159**.

9 X. Xu, K. Shuai and B. Xu, Review on Copper and Palladium Based Catalysts for Methanol Steam Reforming to Produce Hydrogen, *Catalysts*, 2017, **7**, 183, DOI: **10.3390/catal7060183**.

10 A. Iulianelli, P. Ribeirinha, A. Mendes and A. Basile, Methanol steam reforming for hydrogen generation *via* conventional and membrane reactors: A review, *Renew.*

Sustain. Energy Rev., 2014, **29**, 355–368, DOI: 10.1016/j.rser.2013.08.032.

11 R. E. Rosli, A. B. Sulong, W. R. W. Daud, M. A. Zulkifley, T. Husaini, M. I. Rosli, E. H. Majlan and M. A. Haque, A review of high-temperature proton exchange membrane fuel cell (HT-PEMFC) system, *Int. J. Hydrogen Energy*, 2017, **42**, 9293–9314, DOI: 10.1016/j.ijhydene.2016.06.211.

12 L. Piccirilli, D. Lobo Justo Pinheiro and M. Nielsen, Recent Progress with Pincer Transition Metal Catalysts for Sustainability, *Catalysts*, 2020, **10**, 773, DOI: 10.3390/catal10070773.

13 E. Alberico, A. J. J. Lennox, L. K. Vogt, H. Jiao, W. Baumann, H.-J. Drexler, M. Nielsen, A. Spannenberg, M. P. Checinski, H. Junge and M. Beller, Unravelling the Mechanism of Basic Aqueous Methanol Dehydrogenation Catalyzed by Ru–PNP Pincer Complexes, *J. Am. Chem. Soc.*, 2016, **138**, 14890–14904, DOI: 10.1021/jacs.6b05692.

14 M. Nielsen, E. Alberico, W. Baumann, H.-J. Drexler, H. Junge, S. Gladiali and M. Beller, Low-temperature aqueous-phase methanol dehydrogenation to hydrogen and carbon dioxide, *Nature*, 2013, **495**, 85–89, DOI: 10.1038/nature11891.

15 C. H. Schwarz, A. Agapova, H. Junge and M. Haumann, Immobilization of a selective Ru-pincer complex for low temperature methanol reforming–Material and process improvements, *Catal. Today*, 2020, **342**, 178–186, DOI: 10.1016/j.cattod.2018.12.005.

16 C. H. Schwarz, D. Kraus, E. Alberico, H. Junge and M. Haumann, Immobilized Ru-Pincer Complexes for Continuous Gas-Phase Low-Temperature Methanol Reforming-Improving the Activity by a Second Ru-Complex and Variation of Hydroxide Additives, *Eur. J. Inorg. Chem.*, 2021, **2021**, 1745–1751, DOI: 10.1002/ejic.202100042.

17 A. Agapova, H. Junge and M. Beller, Developing Bicatalytic Cascade Reactions: Ruthenium-catalyzed Hydrogen Generation From Methanol, *Chem.–Eur. J.*, 2019, **25**, 9345–9349, DOI: 10.1002/chem.201900966.

18 C. H. Schwarz, Methanol-Dampfreformierung an Geträgerten Homogenen Katalysatoren, PhD thesis, Friedrich-Alexander-Universität Erlangen-Nürnberg, 2021, https://open.fau.de/handle/openfau/16666.

19 H. Li, H. Tian, S. Chen, Z. Sun, T. Liu, R. Liu, S. Assabumrungrat, J. Saupsor, R. Mu, C. Pei and J. Gong, Sorption enhanced steam reforming of methanol for high-purity hydrogen production over Cu-MgO/Al2O3 bifunctional catalysts, *Appl. Catal., B*, 2020, **276**, 119052, DOI: 10.1016/j.apcatb.2020.119052.

20 Q. Guo, Y. Wang, W. Li, Y. Zou and S. Zhang, Oxygen vacancy of Pt/CeO2 enabled low-temperature hydrogen generation from methanol and water, *J. Catal.*, 2024, **430**, 115309, DOI: 10.1016/j.jcat.2024.115309.

21 V. Shanmugam, S. Neuberg, R. Zapf, H. Pennemann and G. Kolb, Hydrogen production over highly active Pt based catalyst coatings by steam reforming of methanol: Effect of support and co-support, *Int. J. Hydr. Energ.*, 2020, **45**, 1658, DOI: 10.1016/j.ijhydene.2019.11.015.

22 Y. Khani, N. Safari, N. Kamyar, F. Bahadoran and M. Torabi, High H2 selectivity with low coke formation for methanol steam reforming over Cu/Y1.5Ce0.84Ru0.04O4 catalyst in a microchannel plate reactor, *Int. J. Hydr. Energ.*, 2022, **47**, 971, DOI: 10.1016/j.ijhydene.2021.10.089.

23 N. Kamyar, Y. Khani, M. M. Amini, F. Bahadoran and N. Safari, Copper-based catalysts over A520-MOF derived aluminum spinels for hydrogen production by methanol steam reforming: The role of spinal support on the performance, *Int. J. Hydr. Energ.*, 2020, **45**, 21341, DOI: 10.1016/j.ijhydene.2020.05.184.

24 G. Chen, Q. Shen, X. Zhang, T. Zhao, K. Zhu and S. Li, High purity H2 resource from methanol steam reforming at low-temperature by spinel CuGa2O4 catalyst for fuel cell, *Ceram. Intern.*, 2024, **50**, 49759, DOI: 10.1016/j.ceramint.2024.09.319.

25 B. Najafi, A. Haghighat Mamaghani, F. Rinaldi and A. Casalegno, Optimization of an HT-PEM fuel cell based residential micro combined heat and power system: A multi-objective approach, *Energy Convers. Manag.*, 2018, **174**, 393, DOI: 10.1016/j.enconman.2018.08.043.

26 Q. Li, R. He, J.-A. Gao, J. O. Jensen and N. J. Bjerrum, The CO poisoning effect in PEMFCs operational at temperatures up to 200 °C, *J. Electrochem. Soc.*, 2003, **150**, A1599, DOI: 10.1149/1.1619984.

27 Q. Li, J. O. Bjerrum, R. F. Savinell and N. J. Bjerrum, High temperature proton exchange membranes based on polybenzimidazoles for fuel cells, *Prog. Polym. Sci.*, 2009, **34**, 449, DOI: 10.1016/j.progpolymsci.2008.12.003.

28 Y. Lwin, Hydrogen production from steam–methanol reforming: thermodynamic analysis, *Int. J. Hydrogen Energy*, 2000, **25**, 47–53, DOI: 10.1016/S0360-3199(99)00013-0.

